International Journal of Microwave and Wireless Technologies

cambridge.org/mrf

FDTD-based SAR calculation of a wearable antenna for wireless body area network devices

Hüseyin Şerif Savcı[1,2] and Fatih Kaburcuk[3]

[1]Electrical and Electronics Engineering Department, College of Engineering and Natural Sciences, Istanbul Medipol University, Istanbul, Turkey; [2]Tubitak Bilgem, Gebze, Turkey and [3]Electrical and Electronics Engineering Department, Sivas Cumhuriyet University, Sivas, Turkey

Research Paper

Cite this article: Savcı HŞ, Kaburcuk F (2023). FDTD-based SAR calculation of a wearable antenna for wireless body area network devices. *International Journal of Microwave and Wireless Technologies* **15**, 1354–1360. https://doi.org/ 10.1017/S1759078722001283

Received: 15 August 2021
Revised: 27 October 2022
Accepted: 28 October 2022

Key words:
Antenna on textile; finite difference time domain (FDTD); specific Absorption rate (SAR); wearable antennas; wireless body area network

Author for correspondence:
Hüseyin Şerif Savcı,
E-mail: hsavci@medipol.edu.tr

Abstract

Wireless-connected wearable electronics are finding extensive usage for diagnostic and therapeutic purposes after the globally spread pandemic disease of COVID-19. Although they are undoubtedly helpful for keeping physical distance, their health effects are still under investigation from different aspects and are still a concern for the end-users. In this study, a custom M-shaped wearable antenna covering the wireless body area network and wireless local area network frequencies is designed, built, and measured. A beret cap made from a 2 mm thick textile is used as a substrate. The specific absorption rate (SAR) in a realistic human-head model due to electromagnetic energy produced by the antenna is evaluated using the finite-difference time-domain method. The SAR distributions for 1-g and 10-g tissues are calculated at 2.4 and 5.8 GHz. It is shown that the obtained maximum SAR values for 1-g and 10-g tissues at each frequency of interest were less than the limits determined by IEEE RF exposure guidelines and standards.

Introduction

The advancement of low-power wireless communication technology in the past couple of decades enabled its utilization in many applications as personal electronics. Personal medical devices are one of the pioneer beneficiaries of their usage. Upon the recommendation of ITU-R in 1999, FCC allocated 402–405 MHz as the Medical Implant Communication Service band in 2001 for the indoor wireless link of medical devices used in diagnostic and therapeutic operations [1]. Since then, numerous implantable, *in-vitro* and wearable medical devices such as cardiac pacemakers, endoscopic camera capsules, cochlear implants, and neuro-stimulators have utilized this band for wireless communication. In addition, semiconductor companies such as Microsemi (back then Zarlink) developed commercially available CMOS-integrated transceivers for both implant modules (ZL70323MNJ) and base station modules (ZL70123MNG7) tailored for MICS applications only. These systems use different antennas, depending on the specific application [2]. MICS base stations generally use helical antennas while the implants incorporate printed antennas such as a meandered planar inverted-F antenna [3], an L-shaped T-line-fed anti-spiral resonator [4], and a commercially available grounded-line technique-based Splatch by antenna factor [5].

Over the years, the increased application complexity, the push for smaller and faster devices, and the addition of more wireless nodes required allocating broader frequency bandwidth and forming a standard. In 2012, FCC allocated 40 MHz of spectrum at 2360–2400 MHz band to medical wireless body area networks (WBANs) as a secondary basis user for short-range indoor low-power wireless links. IEEE 802.15.6 communication standard is established for these body area network devices and can operate with data rates up to 10 Mbps [6].

Besides the medical purpose [7], the wearable body area network devices found applications in many areas such as mobile communications [8] and military [9]. With the introduction of IEEE 802.15.6 in 2012, body-worn WBAN devices such as Google Glass, GoPro cameras, and Nike+ sensor became part of daily life for various applications ranging from remote health monitoring to outdoor sports activity. Such devices utilize antennas strapped or placed on the user, and having an efficient antenna is critical for system performance. Depending on the applications, these systems may require antennas in different shapes, forms, and materials. For example, printing the antenna on textile clothes became a preferred method for most wearable electronics. These antennas must be flexible, low-cost, lightweight, and easy to implement on clothes.

During the fight against the globally spread pandemic COVID-19 disease in the first half of 2020, we, the engineers and medical professionals were seeking the best solution for remote connected and disposable medical sensors. The low-cost wearable wireless medical devices are a good fit for such purposes. Many of these devices do employ printed antennas on textiles for wireless connection. These wearable antennas are usually placed near the human head,

torso, or arm. The antenna's performance is greatly affected by the presence of lossy human tissues inside the antenna's near-field region. In addition to the degradation of antenna performance, the electromagnetic (EM) radiations from the antennas may produce a detrimental effect on the human body [10]. Because many wearable antennas are used for therapeutic, diagnostic, or healthy lifestyle purposes, they are expected not to pose any discomfort to the users. Therefore, it is vital to keep the rate of EM energy absorbed by human tissues below a certain level. This rate is defined as the specific absorption rate (SAR), which must be less than 1.6 W/kg [11] for 1-g of tissues and 2 W/kg [12] for 10-g of tissues.

The SAR distribution in the human head due to EM energy radiated by an adjacent cellular phone having different types of antennas has been studied extensively using the finite-difference time-domain (FDTD) method in [13–23]. In [24–34], the SAR distribution on the part of human body phantom due to a wearable textile antenna has been studied using commercial software tools. In this work, the SAR calculations are performed on a realistic human-head model instead of a rough human body model using our in-house developed custom FDTD Matlab codes [35]. The interaction between a human-head model and a wearable textile antenna has never been evaluated because the FDTD method requires excessively long computation times and large memory requirements when the FDTD cell size is in the order of 0.05 of the wavelength in the tissue. This study utilizes a high-performance computing system to investigate the interaction between a wearable textile antenna and a realistic human-head model with a cell size of 0.5 mm.

In this paper, an M-shaped dual-resonance wearable antenna is designed using the FDTD method and fabricated on a thick textile mat: a skin cap. The fabricated dual-band wearable antenna operates at the WBAN band and 5.8 GHz ISM band, achieving the bandwidth requirements of 40 and 150 MHz, respectively. The antenna performance is evaluated based on two primary performance metrics: the radiation pattern and the input reflection coefficient. These evaluations are done with and without a human-head model. The effect of the EM energy radiated by the wearable antenna based on the SAR distribution in a realistic human-head model is investigated numerically using the in-house developed Matlab codes based on the FDTD method.

Method and models

FDTD method

The FDTD method [35] is one of the most powerful and widely used methods for bio-EM applications due to its ability to handle complex and heterogeneous geometries and provide solutions over a wide band. The FDTD method solves Maxwell's equations in the time domain and calculates the model's six vector components of electric and magnetic fields in each cubic cell. The major constraint [35] in the FDTD method is the cell size, which must be 20 times smaller than the smallest wavelength in the model. Finally, the convolution perfect matching layer (CPML) [36] is applied as an absorbing boundary to truncate the problem domain. In this work, a custom FDTD code is developed to analyze the EM interaction between the realistic human-head model and the designed wearable antenna on a beret cap.

M-shaped wearable antenna on a textile substrate

The top and bottom views of the M-shaped antenna with all dimensions are shown in Fig. 1. A partial ground backs the

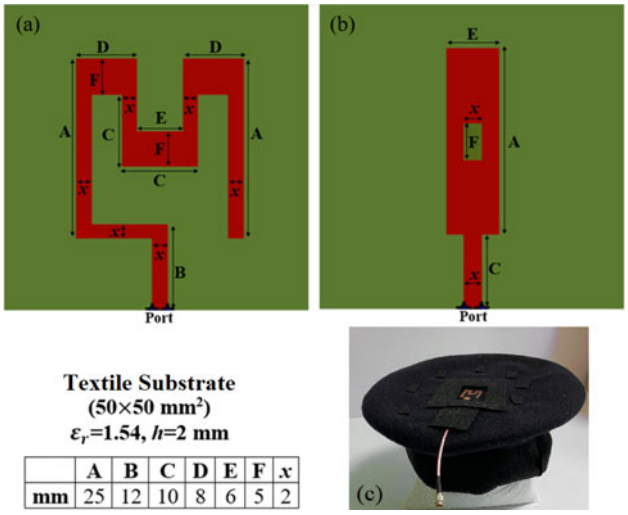

	A	B	C	D	E	F	x
mm	25	12	10	8	6	5	2

Fig. 1. (a) Top and (b) bottom views of the M-shaped wearable antenna with all dimensions, and (c) the fabricated wearable antenna on a flat top textile beret model.

M-shaped driven element on the bottom of the textile material with a slot. The antenna designed using the FDTD method is fabricated on a 2 mm thick textile substrate of dielectric constant $\epsilon_r = 1.54$ with negligible loss. The photograph of the fabricated M-shaped antenna on a beret cap is shown in Fig. 1. The simulation and measurement input reflection coefficients (S_{11}) of the wearable antenna are shown in Fig. 2. It can be seen from the plot that the dual-band resonant frequencies showed a good agreement between the simulation and measurement.

Human-head model

A realistic human-head model proposed in [37] is used in this work. The dimensions of the head model are $172 \times 218 \times 240$ mm^3. The head model is divided into 73 million cells whose sizes in all directions are 0.5 mm. Thus, the total cell number of the FDTD problem space with 10 CPML cells and 10 air gap cells on all sides is about 100 million.

The head model consists of eight tissues: skin, fat, bone, eye, blood vessel, muscle, white matter, and gray matter. The mass density [20], relative permittivity, and conductivity of the head tissues calculated from Debye coefficients in [20] and [38] for 2.4 and 5.8 GHz are tabulated in Tables 1 and 2. Figure 3 shows the human-head model's x–y, x–z, and y–z cross sections.

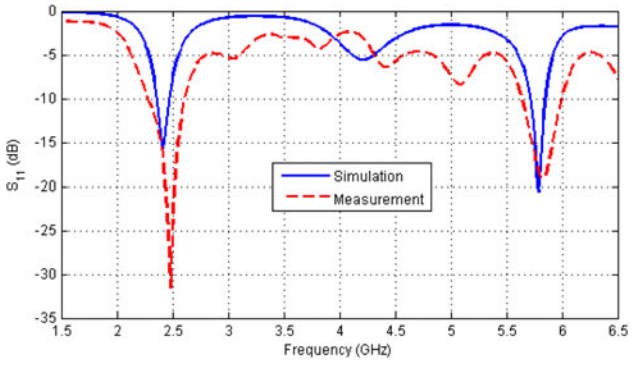

Fig. 2. Simulated and measured S_{11} of the antenna on a textile substrate.

https://doi.org/10.1017/S1759078722001283 Published online by Cambridge University Press

Table 1. Mass density, relative permittivity, and conductivity of the head tissues for 2.4 GHz

Tissues	Mass density	Permittivity	Conductivity
Skin	1125	38.08	1.43
Fat	916	11.44	0.19
Bone	1810	12.41	0.31
Muscle	1047	54.11	1.50
Blood	1058	60.06	2.26
Eye	1100	45.91	1.30
W. matter	1038	37.13	1.05
G. matter	1038	50.28	1.58

Table 2. Relative permittivity and conductivity of the head tissues for 5.8 GHz

Tissues	Permittivity	Conductivity
Skin	35.11	3.72
Fat	11.01	0.71
Bone	11.21	1.16
Muscle	51.56	4.51
Blood	56.35	6.08
Eye	43.44	4.02
W. matter	34.74	3.24
G. matter	46.98	4.63

SAR calculation

The EM energy absorbed by biological tissues is quantified as SAR. The SAR is defined as

$$SAR(r) = \sigma(r)E(r)/2\rho(r)$$

where E is the root-mean-square magnitude of the electric field strength in V/m, σ is the conductivity of tissue, ρ is the mass density of the tissue, and r denotes the indexed cell. The IEEE standard C95.3-2002 [39] is used to calculate the SAR distributions over 1-g of tissue (SAR_{1g}) and 10-g of tissue (SAR_{10g}) in the human head model. The input power of the antenna for

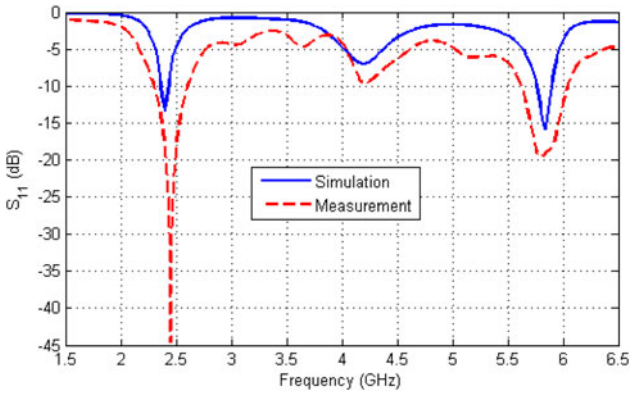

Fig. 4. Simulated and measured S_{11} of the wearable antenna with the human-head model.

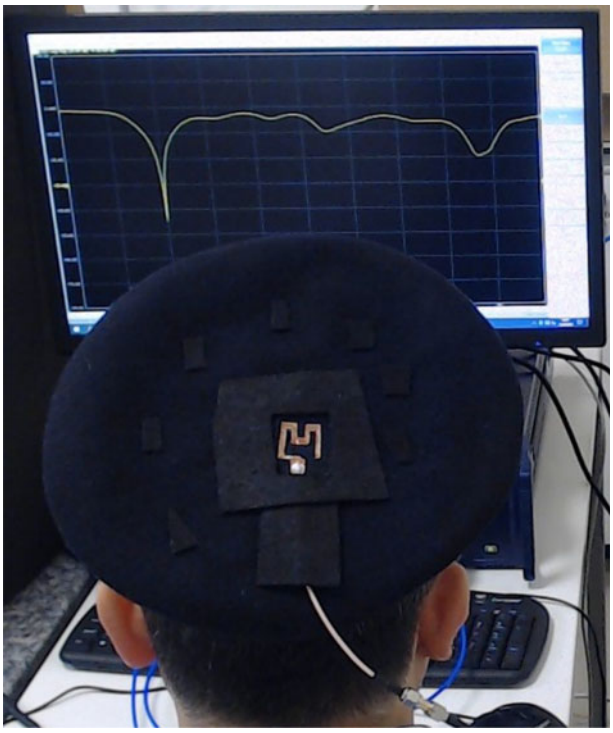

Fig. 5. Photograph of the wearable antenna with a real human head.

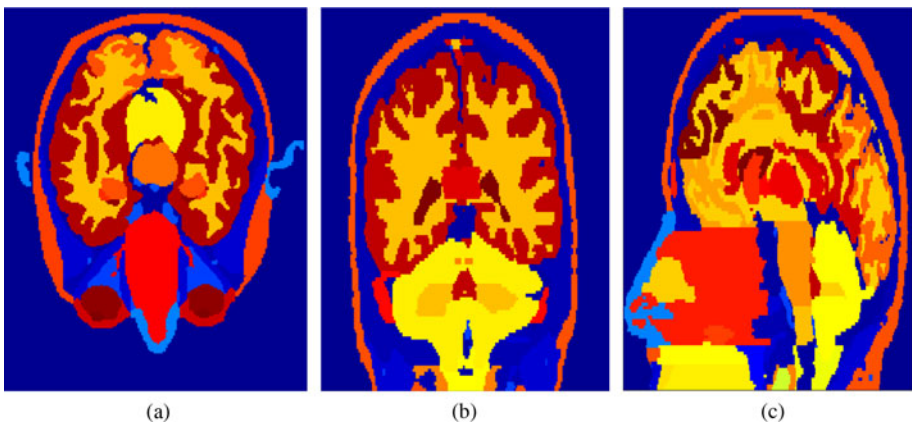

Fig. 3. (a) *x*–*y*, (b) *x*–*z*, (c) and *y*–*z* cross-sections of the human-head model.

https://doi.org/10.1017/S1759078722001283 Published online by Cambridge University Press

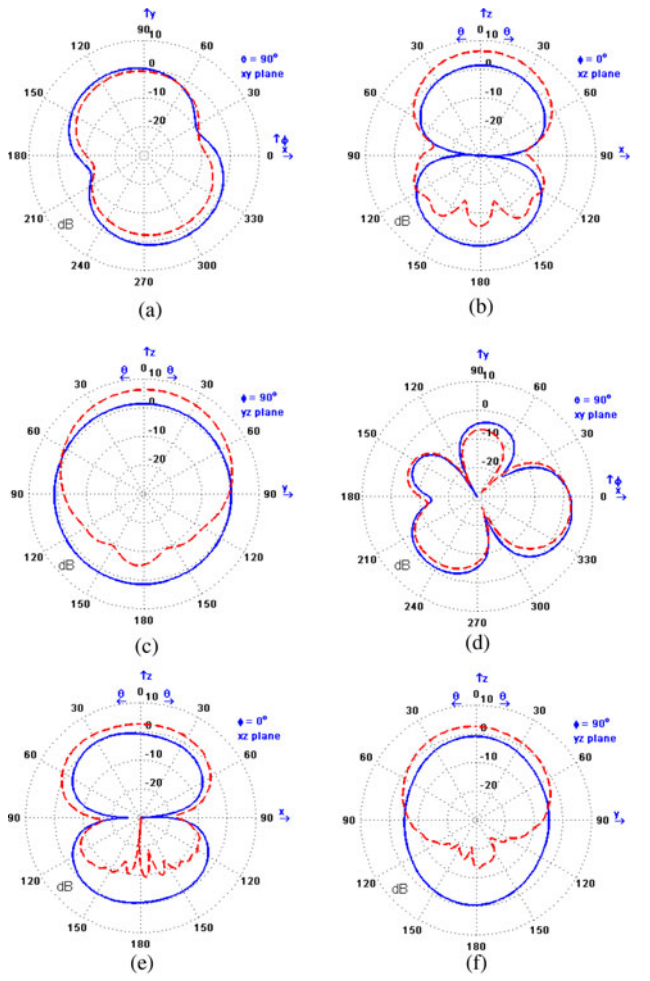

Fig. 6. Radiation patterns of the wearable antenna with and without human-head model on the (a) the *x*–*y*, (b) the *x*–*z*, and (c) the *y*–*z* plane cuts for 2.4 GHz and (d) the *x*–*y*, (e) the *x*–*z*, and (f) the *y*–*z* plane cuts for 5.8 GHz (blue curves: only antenna; red dashed curves: head with the antenna).

2.4 and 5.8 GHz is set to 20 dBm, which is the maximum power of wireless local area networks (WLANs). The assumption of being exposed to such a power rating is realistic when the co-existence of WLAN and WBAN in a medical environment is considered.

Numerical results

This section investigates the effects of the human-head model on the input reflection coefficient and the wearable antenna's radiation patterns. Then, the EM effect of the wearable antenna fabricated on the beret cap to the human-head model is investigated at 2.4 and 5.8 GHz by using the FDTD

Table 3. Maximum gain (gain) and efficiency (eff.) of the antenna with and without the head at 2.4 and 5.8 GHz

	2.4 GHz		5.8 GHz	
	Gain	Eff.	Gain	Eff.
Antenna w/o head	1.69	75	4.12	83
Antenna w/ head	6.20	68	2.96	57

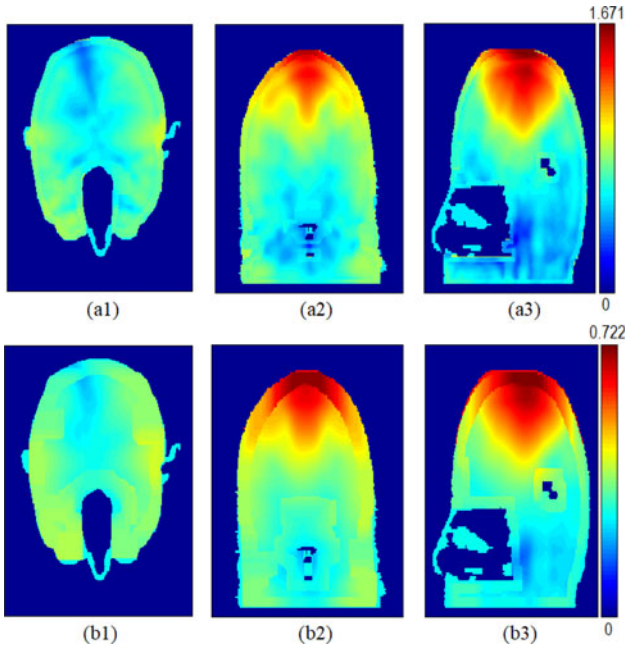

Fig. 7. (a1), (a2), (a3) SAR_{1g} and (b1), (b2), (b3) SAR_{10g} (W/kg) distributions on the *x*–*y*, *x*–*z*, and *y*–*z* cross sections of the human-head model for 2.4 GHz.

numerical solution. The SAR_{1g} and SAR_{10g} distributions in the human-head model due to the wearable antenna are calculated at each frequency of interest. The FDTD numerical problem is constructed with the antenna printed on a textile beret model placed 12 mm above the human-head model. Matlab-based custom-developed FDTD codes are used in this study. The simulations are done in the 2018 64-bit Matlab version running on a 32-core high-power computing system with 512 GB RAM. The computation time for the entire

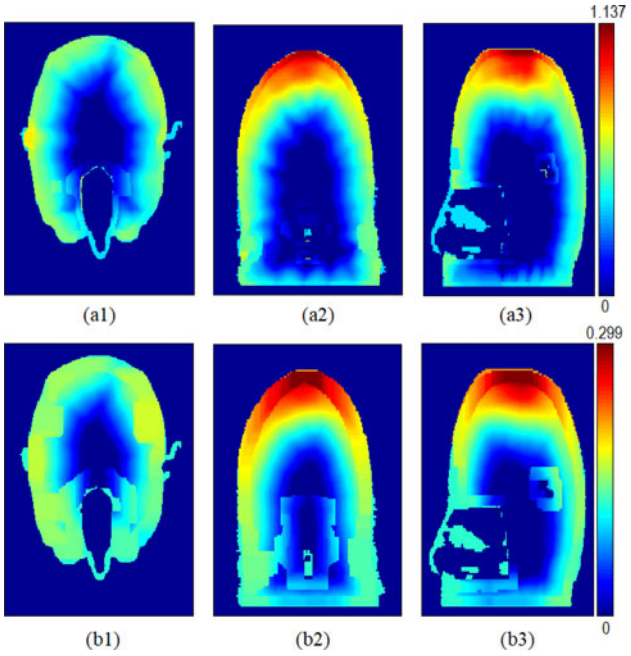

Fig. 8. (a1), (a2), (a3) SAR_{1g} and (b1), (b2), (b3) SAR_{10g} (W/kg) distributions on the *x*–*y*, *x*–*z*, and *y*–*z* cross sections of the human-head model for 5.8 GHz.

https://doi.org/10.1017/S1759078722001283 Published online by Cambridge University Press

Table 4. Maximum SAR_{1g} and SAR_{10g} at 2.4 and 5.8 GHz

	2.4 GHz	5.8 GHz
SAR_{1g} (W/kg)	1.671	1.137
SAR_{10g} (W/kg)	0.722	0.299

Table 5. Design features of some recent studies in the literature

Ref.	Substrate	Thickness (mm)	Phantom model	Antenna location
[40]	Denim	0.7	Sphere	Leg
[41]	Composite	1.5	Voxel	Wrist
[42]	Latex	4	Voxel	Chest
[28]	Felt	6	Voxel	Chest
[43]	Textile	3	Cubic	Wrist
[32]	Kevlar	2.6	Voxel	Arm
[44]	Metasurfaces	3	Cubic	Chest
This study	Textile	2	Voxel	Head

EM analysis and the SAR calculations is roughly 12 000 min. The solution is done without any simplification and mesh optimization. The CPU-based numerical solution for such a big problem would be incredibly long on a standard workstation. For such reason, this study would be a reference for simplified solutions.

Effect of human-head model on the antenna performance

The simulations are done with a realistic human-head model, and the measurements are taken while the beret cap is placed on a human head. The superimposed plot having both the simulated and measured input reflection coefficients is shown in Fig. 4. It can be seen from the plot that the simulated and measured performances match pretty well. Our FDTD algorithm is only coded for the use case of a flat antenna substrate and does not cover the case for bent structures. Therefore it is essential to keep the antenna structure flat. The textile material is reinforced from the perimeter of the top surface of the cap to keep the antenna printed region flat while it is worn. The slight deviations in the measured performance are due to the variation in the electrical properties of textile material and fabrication tolerances. Figure 5 shows the photograph taken during the measurements while the textile beret with antenna was worn. The radiation patterns of the wearable antenna with and without the human-head model at resonance frequencies obtained using the FDTD method are shown in Fig. 6. The maximum gain (dBi) and efficiency (%) values of the antenna with and without the head model are tabulated in Table 3.

SAR_{1g} and SAR_{10g} distributions in the human head due to the wearable antenna

The SAR_{1g} and SAR_{10g} distributions in the x–y, x–z, and y–z cross sections of the human head model are shown for 2.4 and 5.8 GHz in Figs 7 and 8, respectively. The maximum values of SAR_{1g} and SAR_{10g} at resonance frequencies are tabulated in Table 4. The SAR_{1g} and SAR_{10g} values reported in Table 4, except the value at 2.4 GHz, are less than 1.6 W/kg [11] for 1-g of tissues and 2 W/kg [12] for 10-g of tissue, respectively. At 2.4 GHz, the maximum SAR_{1g} value just above 1.6 W/kg is within an acceptable range according to the studies in the literature. It can be seen from Figs 7 and 8 that the maximum SAR values occur on the top of the human head due to the wearable antenna on the flat top textile beret. It is also realized from these figures the SAR_{1g} and SAR_{10g} distributions appear in a good correlation. It can be realized that the resonance frequencies affect the maximum SAR_{1g} and SAR_{10g} values and SAR distributions.

Calculation of the SAR distributions on the human body parts due to a wearable textile antenna by using commercial software tools is the prime topic of antenna research [24–34] in recent years. A fair comparison of the obtained results is difficult because the SAR distributions and maximum SAR values depend on antenna types, substrates, input power, resonance frequencies, and distance between the antenna and the human body phantom.

Textile antennas on the human body model have been reported in [28, 32, 40–44]. Tables 5 and 6 summarize the existing studies regarding design features (substrate type and thickness, location on the human body model, and phantom model) and performance metrics (antenna resonance frequencies, gain, input power, SAR_{1g}, and SAR_{10g} values), respectively. The tables show that the antenna's properties, input power, and phantom model affect the maximum SAR values.

Conclusion

The need for remote health operations is increased tremendously over the last 2 years due to the global spread of pandemic diseases.

Table 6. Performance comparison of some recent studies in the literature

Ref.	Frequency (GHz)	Gain (dBi)	Power (dBm)	SAR_{1g} (W/kg)	SAR_{10g} (W/kg)
[40]	2.4	7.8	20	0.29	–
[41]	2.44	5.1	20	0.18	–
[42]	2.45	5	30	1.47	0.71
[28]	2.45–5.2	−3.5 to 6.6	27	0.4–0.7	–
[43]	2.45–5.5	−0.7 to 7.4	23	0.48–0.02	–
[32]	1.58–2.45	2–2	20	0.78–0.71	–
[44]	2.45	4.3	23	0.65	–
This study	2.4–5.8	6.2–3.0	20	1.67–1.14	0.72–0.3

https://doi.org/10.1017/S1759078722001283 Published online by Cambridge University Press

The low-cost wearable RF devices find wide usage for diagnostic and therapeutic purposes. In such cases, it would be a significant question to answer if the wearable devices pose any discomfort or health risk to the patients. In this study, the interactions between a realistic human-head model and RF EM fields radiated by a wearable antenna were evaluated using the FDTD method at WBAN and WLAN frequencies. A custom M-shaped antenna is designed on a beret made out of textiles. The fabric is characterized as a 2 mm thick substrate. The antenna is manufactured and measured in our RF lab. The simulation and measurement results show a good agreement. Then, the effect of the wearable antenna, the SAR_{1g}, and SAR_{10g} distributions on the human head are calculated using the FDTD method. Based on this study, it is concluded that even under maximum WLAN power settings, the SAR ratings of the wearable antenna designed for this study are still under the IEEE maximum RF exposure limits.

Conflict of interest. None.

References

1. **Savci HS, Sula A, Wang Z, Dogan NS and Arvas E** (2005) MICS transceivers: regulatory standards and applications. In *IEEE SoutheastCon, 2005*, Fort Lauderdale, FL, USA, pp. 179–182.
2. **Basmer T, Todtenberg N, Popiella F and Birkholz M** (2013) Antennas for medical implant applications operating in the MICS band. In *IEEE MTT-S International Microwave Workshop Series on RF and Wireless Technologies for Biomedical and Healthcare Applications (IMWS-Bio 2013)*, Singapore.
3. **Lee JH, Seo DW and Lee HS** (2015) Design of implantable antenna on the dielectric/ferrite substrate for wireless biotelemetry. In *2015 International Symposium on Antennas and Propagation (ISAP)*, Hobart, TAS, pp. 1–3.
4. **Palandoken M** (2017) Compact bioimplantable MICS and ISM band antenna design for wireless biotelemetry applications. *Radioengineering* **26**, 917–923.
5. **Datasheet**(2017) ANT-403-SP: The Splatch, Rev 11-11-08ANT. Linx Technologies.
6. **IEEE Standard** (2012) IEEE standard for local and metropolitan area networks – part 15.6: Wireless Body Area Networks. IEEE Computer Society, IEEE Standard 802.15.6-2012, pp. 1-271, 29 Feb. 2012.
7. **Sabban A** (2013) New wideband printed antennas for medical applications. *IEEE Transactions on Antennas and Propagation* **61**, 84–91.
8. **Rogier H, Agneessens S, Castel T, Lemey S, Declercq F, Vanveerdeghem P, Van Torre P, Vallozzi L and Joseph W** (2014) Novel wearable antenna systems for high data rate mobile communication in healthcare. In *4th International Conference on Wireless Mobile Communication and Healthcare – Transforming Healthcare Through Innovations in Mobile and Wireless Technologies (MOBIHEALTH)*, Athens, pp. 188–191.
9. **Lee H, Tak J and Choi J** (2017) Wearable antenna integrated into military berets for indoor/outdoor positioning system. *IEEE Antennas and Wireless Propagation Letters* **16**, 1919–1922.
10. **Hardell L and Sage C** (2008) Biological effects from electromagnetic field exposure and public exposure standards. *Biomedicine & Pharmacotherapy* **62**, 104–109.
11. **Ulcek J and Cleveland RF** (1997) Evaluating compliance with FCC guidelines for human exposure to radio frequency electromagnetic fields. Supplement B to Federal Communications Commission OET Bulletin 65 (Edition 97-10).
12. **IEEE Standard** (2016) IEEE C95.1. IEEE standard for safety levels concerning human exposure to radio frequency electromagnetic fields, 3 kHz to 300 GHz. IEEE Standard C95.1-2005.
13. **Wang J and Fujiwara O** (1999) FDTD computation of temperature rise in the human head for portable telephones. *IEEE Transactions on Microwave Theory and Technique* **47**, 1528–1534.
14. **Bernardi P, Cavagnaro M, Pisa S and Piuzzi E** (2001) Power absorption and temperature elevations induced in the human head by a dual-band monopole-helix antenna phone. *IEEE Transactions on Microwave Theory and Technique* **49**, 2539–2546.
15. **Hirata A and Shiozawa T** (2003) Correlation of maximum temperature increase and peak SAR in the human head due to handset antennas. *IEEE Transactions on Microwave Theory and Technique* **51**, 1834–1841.
16. **Hirata A, Morita M and Shiozawa T** (2003) Temperature increase in the human head due to a dipole antenna at microwave frequencies. *IEEE Transactions on Electromagnetic Compatibility* **45**, 109–116.
17. **Fujimoto M, Hirata A, Wang JQ, Fujiwara O and Shiozawa T** (2006) FDTD-derived correlation of maximum temperature increase and peak SAR in child and adult head models due to dipole antenna. *IEEE Transactions on Electromagnetic Compatibility* **48**, 240–247.
18. **Hirata A, Shirai K and Fujiwara O** (2008) On averaging mass of SAR correlating with temperature elevation due to a dipole antenna. *Progress in Electromagnetics Research* **84**, 221–237.
19. **Islam MR and Ali M** (2013) Temperature rise induced by wire and planar antennas in a high-resolution human head model. *IEEE Transactions on Electromagnetic Compatibility* **55**, 288–298.
20. **Kaburcuk F and Elsherbeni AZ** (2018) Temperature rise and SAR distribution at wide range of frequencies in a human head due to an antenna radiation. *Applied Computational Electromagnetics Society Journal* **33**, 367–372.
21. **Kaburcuk F** (2019) Effects of a brain tumor in a dispersive human head on SAR and temperature rise distributions due to RF sources at 4G and 5G frequencies. *Electromagnetic Biology and Medicine* **38**, 168–176.
22. **Kaburcuk F and Elsherbeni AZ** (2021) Efficient electromagnetic analysis of a dispersive head model due to smart glasses embedded antennas at Wi-Fi and 5G frequencies. *Applied Computational Electromagnetics Society Journal* **36**, 159–167.
23. **Geyikolu MD, Kaburcuk F and Çavusolu B** (2020) SAR analysis of triband antennas for a 5G eyewear device. *International Journal of Microwave and Wireless Technologies* **12**, 754–761.
24. **Salonen P, Rahmat-Samii Y and Kivikoski M** (2004) Wearable antennas in the vicinity of human body. *IEEE Antennas and Propagation Society Symposium* **1**, 467–470.
25. **Jalil ME, Abdul Rahim MK, Samsuri NA, Murad NA, Othman N and Majid HA** (2013) On-body investigation of dual band diamond textile antenna for wearable applications at 2.45 GHz and 5.8 GHz. In *2013 7th European Conference on Antennas and Propagation (EuCAP)*. Gothenburg, Sweden: IEEE, pp. 414–417.
26. **Al-Ashwal WAM and Ramli KN** (2013) Compact UWB wearable antenna with improved bandwidth and low SAR. In *2013 IEEE International RF and Microwave Conference (RFM)*. Penang, Malaysia: IEEE, pp. 90–94.
27. **Al-Ashwal WAM and Ramli KN** (2014) Small planar monopole UWB wearable antenna with low SAR. In *2014 IEEE Region 10 Symposium*, pp. 235–239.
28. **Yan S, Soh PJ and Vandenbosch GAE** (2015) Compact all-textile dual-band antenna loaded with metamaterial-inspired structure. *IEEE Antennas and Wireless Propagation Letters* **14**, 1486–1489.
29. **Ramli MN, Soh PJ, Abdul Rahim H, Jamlos MF, Giman FN, Hussin EFNM, Lago H and Van Lil E** (2017) SAR for wearable antennas with AMC made using PDMS and textiles. *2017 XXXIInd General Assembly and Scientific SympoRFum of the International Union of Radio Science (URSI GASS)*, 1–3.
30. **Simorangkir RBVB, Yang Y, Matekovirs L and Esselle KP** (2017) Dual-band dual-mode textile antenna on PDMS substrate for bodycentric communications. *IEEE Antennas and Wireless Propagation Letters* **16**, 677–680.
31. **Atrash ME, Abdalla MA and Elhennawy HM** (2019) A wearable dual-band low profile high gain low SAR antenna AMC-back for WBAN applications. *IEEE Transactions on Antennas and Propagation* **67**, 6378–6388.
32. **Joshi R, Hussin EFNM, Soh PJ, Jamlos MF, Lago H, Al-Hadi AA and Podilchak SK** (2020) Dual-band, dual-sense textile antenna with AMC backing for localization using GPS and WBAN/WLAN. *IEEE Access* **8**, 89468–89478.

https://doi.org/10.1017/S1759078722001283 Published online by Cambridge University Press

33. **Le TT and Yun TY** (2020) Miniaturization of a dual-band wearable antenna for WBAN applications. *IEEE Antennas Wireless Propagation Letters* **19**, 1452–1456.
34. **Le TT and Yun TY** (2021) Wearable dual-band high-gain low-SAR antenna for off-body communication. *IEEE Antennas and Wireless Propagation Letters* **20**, 1175–1179.
35. **Elsherbeni AZ and Demir V** (2016) *The Finite-Difference Time-Domain Method for Electromagnetics with MATLAB Simulations*, 2nd Ed., ACES Series on Computational Electromagnetics and Engineering. Edison, NJ: SciTech Publishing.
36. **Roden JA and Gedney SD** (2000) Convolution PML (CPML): an efficient FDTD implementation of the CFS-PML for arbitrary media. *Microwave and Optical Technology Letters* **27**, 334–339.
37. **Zubal IG, Harrell CR, Smith EO, Rattner Z, Gindi GR and Hoffer PB** (1994) Computerized three-dimensional segmented human anatomy. *Medical Physics* **21**, 299–302.
38. **Eleiwa MA and Elsherbeni AZ** (2001) Debye constants for biological tissues from 30 Hz to 20 GHz. *ACES Journal* **18**, 202–213.
39. **IEEE Standard** (2002) IEEE recommended practice for measurements and computations of radio frequency electromagnetic fields with respect to human exposure to such fields. 100 kHz–300 GHz. IEEE Standard C95.3-2002, Annex E.
40. **Ashyap AYI, Abidin ZZ, Dahlan SH, Abdul Majid H, Shah SM, Kamarudin MR and Alomainy A** (2017) Compact and low-profile textile EBG-based antenna for wearable medical applications. *IEEE Antennas and Wireless Propagation Letters* **16**, 2550–2553.
41. **Jiang ZH, Cui Z, Yue T, Zhu Y and Werner DH** (2017) Compact, highly efficient, and fully flexible circularly polarized antenna enabled by silver nanowires for wireless body-area networks. *IEEE Transactions on Biomedical Circuits and Systems* **11**, 920–932.
42. **Agarwal K, Guo Y and Salam B** (2016) Wearable AMC backed near-endfire antenna for on-body communications on latex substrate. *IEEE Transactions on Components, Packaging and Manufacturing Technology* **6**, 346–358.
43. **Zhang K, Soh PJ and Yan S** (2022) Design of a compact dual-band textile antenna based on metasurface. *IEEE Transactions on Biomedical Circuits and Systems* **16**, 211–221.
44. **Zhang K, Vandenbosch GAE and Yan S** (2020) A novel design approach for compact wearable antennas based on metasurfaces. *IEEE Transactions on Biomedical Circuits and Systems* **14**, 918–927.

Hüseyin Şerif Savcı received a BS in Electronics & Communication Engineering from Yildiz Technical University, Istanbul, Turkey, in 2001 and his MS and Ph.D. degrees in Electrical Engineering from Syracuse University, Syracuse, NY, USA, in 2005 and 2008, respectively. His dissertation on low CMOS receiver for medical implant devices was awarded the Syracuse University 2009 best thesis award. From 2008 to 2013, he was with Skyworks Solutions Inc., Cedar Rapids, IA, USA, as a senior RFIC design engineer. Between 2013 and 2020, he worked for Hittite Microwave Corporation, Chelmsford, Massachusetts, and Analog Devices Inc., Istanbul, Turkey, as a principal design engineer, where he designed many RFIC and MMIC products on SOI, GaN, and GaAs technologies for test and measurement, microwave/mm-wave cellular infrastructure, and ADEF applications. In 2020, he joined the Department of Electrical and Electronics Engineering at Istanbul Medipol University, Istanbul, Turkey, as an assistant professor. His research interests include designing and modeling RF and microwave integrated circuits, devices, systems, and antennas. He is serving as an associate editor for the *Applied Computational Electromagnetics Society (ACES) Journal*.

Fatih Kaburcuk received his MS and Ph.D. degrees in Electrical Engineering from Syracuse University, Syracuse, NY, USA, in 2011 and 2014, respectively. During his graduate studies, he worked as a research assistant with Syracuse University and PPC-Belden Inc. in Liverpool, NY, USA. He worked as a visiting research scholar at the Department of Electrical Engineering, Colorado School of Mines, Golden, CO, USA, in 2014. He joined the Erzurum Technical University in 2015 and served as an assistant professor until 2019. Currently, Dr. Kaburcuk has been serving as an associate professor in the Department of Electrical and Electronics Engineering at Sivas Cumhuriyet University, Sivas, Turkey. He is an associate editor for the *Applied Computational Electromagnetics Society (ACES) Journal*. His research interests include numerical methods in electromagnetics, the biological effect of electromagnetic radiation, and finite-difference time-domain analysis of antennas and RF devices.

https://doi.org/10.1017/S1759078722001283 Published online by Cambridge University Press